PAPER

Check for updates

Synergistic or antagonistic effect of lanthanides on Rose Bengal photophysics in upconversion nanohybrids?†

Juan Ferrera-González, [ID] María González-Béjar [ID] * and Julia Pérez-Prieto [ID] *

A nanohybrid made of a xanthenic dye, rose bengal, grafted to an ytterbium and erbium codoped upconversion nanoparticle (UCNP) served as a proof-of-concept to evaluate the fundamental mechanisms which govern the dye photophysics upon interaction with the UCNP. Both photoactive lanthanides strongly influence the singlet and triplet excited states of rose bengal.

Introduction

Upconversion nanoparticles (UCNPs) are nanoparticles able to convert low energy photons into higher energy photons. The process, termed upconversion (UC), occurs due to the unique properties of photoactive lanthanide ions (Ln^{3+}), which are the dopants of a transparent low-phonon energy matrix. UC is a nonlinear phenomenon and, usually, gives rise to multiple long-lifetime narrow emission bands in the ultraviolet–visible–near infrared (UV–vis–NIR) region upon NIR excitation.[1,2]

Furthermore, upconversion nanohybrids (UCNHs), which combine UCNPs and photoactive species (*e.g.*, dyes, organometallic complexes, or other photoactive nanoparticles) have been used for applications as sensors and bioimaging or therapeutic agents (photothermal, photodynamic, chemotherapy, radiotherapy and so on).[3–9] Often, the photophysical interaction of both constituents in the UCNHs gives rise to an additive or synergistic effect to improve the optical features or generate new ones.

Most of the UCNHs reported so far include chromophores (usually organic dyes) and use energy transfer (trivial or resonant) processes which occur from the Ln^{3+} upconversion emission in the UCNP to the chromophore (NIR sensitization of the chromophore) or *vice versa* (dye-sensitized UCNP) by

selective excitation of the desired counterpart.[10–14] Some UCNHs, upon selective excitation of the UCNP and subsequent energy transfer to the chromophore, can generate triplet states after intersystem crossing. This chromophore can then react with oxygen to produce reactive oxygen species (ROS).[4,15] Among the chromophores used to fabricate UCNHs are pyropheophorbide a,[16] cationic porphyrin TMPyP4,[17] diiodo-BODIPY,[18] Rose Bengal (RB),[19] methylene blue,[20] hypericin,[21] chlorine e6,[22] and merocyanine 540.[23]

Great efforts have been made to study, model and improve the energy transfer process from the UCNP Ln^{3+} doping to the chromophore.[11,24–30] More than 5000 research articles about UCNHs composed of UCNPs and dyes have been already published,‡ but only five of them analyzed experimentally the effect of Ln^{3+} on the dye excited state photophysics. It is desirable to gain a deeper understanding of the effect that the photoactive lanthanide doping of the UCNP has on the photophysical properties of chromophores. In this context, it was reported that the presence of heavy lanthanides, in particular Gd^{3+}, in the UCNP favored the intersystem crossing of a dye anchored to the UCNP surface (IR-806) through the heavy atom effect, eventually leading to dye triplet formation.[31] Later, the enhancement of intersystem crossing was confirmed for other lanthanide cations (Tb^{3+}, Eu^{3+}, Gd^{3+} and Yb^{3+}) on films of Ln^{3+}-doped nanoparticles with aromatic molecules; remarkably, this enhancement was not only linked to the heavy atom effect, but also to cations with unpaired 4f electrons (dye photophysics remained identical for Y^{3+} and Lu^{3+} doped nanoparticles). Moreover, heavy lanthanides with

Instituto de Ciencia Molecular (ICMol), Departamento de Química Orgánica, Universitat de València, C/ Catedrático José Beltrán, 2, Paterna, Valencia 46980, Spain. E-mail: maria.gonzalez@uv.es, julia.perez@uv.es

†Electronic supplementary information (ESI) available: Materials and methods, UC_{Er} TEM images, UC_{Er} ICP-MS analysis, absorption of RB, attenuance of UC_{Er}@RB, RB concentration study in DMF, calculation of RB molecules per UCNP, TAS spectra and kinetics of RB and UC_{Er}@RB, scheme of RB photophysical processes under N_2 and air, $k_q(O_2)$ Stern–Volmer plot, NIR-II emission kinetics, upconversion and downshifting emission kinetics of UC_{Er} and UC_{Er}@RB and their fitting parameters. See DOI: https://doi.org/10.1039/d3nr03774f

‡ Search performed in Web of Science (Clarivate Analytics) reported 5242 results with the following input data: database: all; type of document: article; topic: upconversion nanoparticles; keywords should include: upconverting nanoparticles, nanohybrid, nanosystem, nanoplatform, nanostructure, heterostructure; keywords must include: dye. Date of search: 2023-10-11.

unpaired electrons also enabled the observation of the triplet exciton absorption transition ($S_0 \rightarrow T_n$) and the triplet state absorption deactivation lifetime decreased with respect to that of the pristine dye due to energy transfer to the Ln^{3+} ions.[32] Afterwards, by knowing the effect that some lanthanides have on the intersystem crossing of dyes, a smart UCNH was developed to enable sensitization of a lanthanide with no intermediate energy levels (Tb^{3+} and Eu^{3+}) in a core–shell–shell UCNH through dye triplet excited states.[33] More recent research attributes, once again, the heavy atom effect as responsible for the intersystem crossing enhancement.[34,35] Although the exact mechanism behind these observations is still controversial, all these publications clearly demonstrate that Ln^{3+} in the UCNP influences the dye photophysics.

Moreover, the restriction of movement of the dye anchored to the surface, the interaction with the surface[36] and the potential dye aggregation[37,38] raise serious doubts as to whether its behavior is the same as when it is free in solution. Consequently, dye photophysics can change considerably and should be reported for each UCNH.

Herein, we have selected a colloidal UCNH, commonly used in the field, as a model to evaluate the photophysical processes and phenomena that take place between its counterparts. Specifically, the UC_{Er}@RB UCNH is composed of β-$NaYF_4$:Yb^{3+}(20%),Er^{3+}(2%), a UCNP of *ca.* 20 nm and RB adsorbed on the surface. UC_{Er}@RB has been selected based on the relatively high resonant energy transfer from Er^{3+} to RB and its reproducible and easy synthesis.[39] In this system, RB absorption overlaps the main UC emission of Er^{3+} (520–540 nm). Moreover, RB photophysics is well known and presents a high intersystem crossing quantum yield (>90%)[40] and $^1O_2$ generation (68–80%).[41]

UCNHs made of UCNPs and RB have been investigated in the past.[19,42–45] Most of them detected $^1O_2$ by using optical probes (*e.g.*, 1,3-diphenylisobenzofuran, DPBF) or by detecting $^1O_2$ phosphorescence.[§,19] Core–shell structures with increased concentrations of donor lanthanides in the shell are beneficial for resonant energy transfer to dyes.[24] Also, the thickness of a silica shell coating the UCNP ($NaYF_4$:Yb^{3+}(20%),Er^{3+}(2%)) influences the energy transfer to RB on the surface.[45] The distance exerted an opposite influence between UC luminescence (reducing surface effects and solvent deactivation) and the energy transfer efficiency. The best energy transfer occurred with a 6 nm coating, leading to an emission of RB sensitized by UCNP with a lifetime on the microsecond scale.

All this considered, there is still an important lack of knowledge about how the photophysics of chromophores can be affected when anchored to the UCNP surface in colloidal dispersions.

This work presents a comparative analysis between free RB and RB in a UCNH and focusses on obtaining the most com-

plete overview of the photophysical processes that could take place between the photoactive counterparts in UC_{Er}@RB. It is of fundamental importance to understand the overall photophysics of the nanohybrid and develop nanomaterials with appropriate photoactive properties.

Does the combination of RB with UCNPs generate a synergistic or an antagonistic effect on RB photophysics in these "well-known" UCNHs?

Results and discussion

Nanohybrid synthesis and characterization

One batch of β-$NaYF_4$:Yb^{3+}(28%),Er^{3+}(3%) UCNPs were synthesized by thermal decomposition (see Table S1†).[46] The hexagonal prisms had a size of 21.0 ± 0.8 × 18.9 ± 0.7 nm (Fig. S1†). Subsequently, the UCNPs were treated with $NOBF_4$ to eliminate oleate ligands from the surface,[47] giving rise to oleate-free UCNPs (UC_{Er}). Then, UC_{Er} was exposed to an excess of RB (42 mM) in DMF under shaking for 24 hours, followed by washing with DMF until the supernatant showed negligible RB absorption. The resulting UCNHs, UC_{Er}@RB, were redispersed in DMF.

Dynamic light scattering (DLS) measurements showed that the average hydrodynamic diameter (D_h) of UC_{Er}@RB increases slightly (either by intensity or number) (Fig. S2:† 27.9 ± 0.3 and 86.3 ± 0.8 nm for UC_{Er} and UC_{Er}@RB, respectively). This reflected the UCNP coverage with the dye. Moreover, the average polydispersity index (PDI) for UC_{Er} and UC_{Er}@RB was 0.238 ± 0.015 and 0.344 ± 0.006, respectively. The acceptable monodispersity of the samples supports that the degree of RB functionalization among UCNPs is fairly homogeneous.

Photophysics of UC_{Er}@RB

The photophysical interaction between UC_{Er} and RB in UC_{Er}@RB has been studied and is presented in the next two sections. *N*,*N*-Dimethylformamide (DMF) has been the solvent of choice because it allows the preparation of concentrated, low-scattering dispersions of UC_{Er}@RB. Fig. 1 shows the energy diagrams for the photophysical processes that can be observed for UC_{Er}@RB exciting either the dye (λ_{exc} = 560 nm) or the UCNP (λ_{exc} = 980 nm).

Photophysics of RB in the UCNH

The photophysical properties of RB in the UC_{Er}@RB dispersion were studied and compared with those of RB in solution to evaluate the effect that aggregation and photoactive lanthanide doping of UC_{Er} have on the photophysical properties of RB. The contribution of each excited state is summarized in Table 1. Energy transfer from RB to UC_{Er} in the UCNH is also discussed.

Ground and singlet states of RB. The absorption and emission spectra of RB and UC_{Er}@RB in DMF are shown in Fig. 2a. Both present the characteristic absorption band with a shoulder, but the absorption band of RB in UC_{Er}@RB is wider than that of RB and the absorption maximum (λ_{max}) under-

---

§ Set up: O_2-saturated D_2O colloidal dispersion with no reported concentration; excitation: a CW 980 nm laser diode with no reported power density; detection: a liquid nitrogen cooled InGaAs detector.
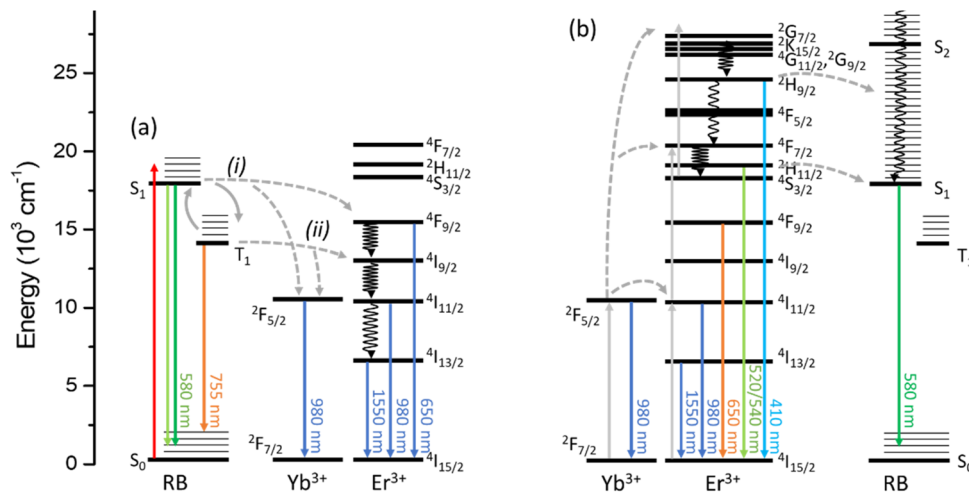
Fig. 1 Energy diagram of photophysical processes observed for $UC_{Er}@RB$ under N_2 exciting the (a) dye (λ_{exc} = 560 nm) or the (b) UCNP (λ_{exc} = 980 nm).

Table 1 Photophysical properties under an N_2 atmosphere (λ_{exc} = 560 nm). Fitting parameters are shown in Table S2†

Sample	$\Phi_F \pm SD^a$	$\tau_F \pm SD^a$ (ns)	$\Phi_{isc} \pm SD$	$\tau_T \pm SD^a$ (μs)	$\tau_{Bl} \pm SD^a$ (μs)	$k_q(O_2)^c \pm SD^a$ (10^8 M^{-1}s^{-1})	I_P (a.u.)	$\tau_P \pm DS^a$ (μs)	I_{DF} (a.u.)
RB	0.420 ± 0.003	2.2 ± 0.1	0.45 ± 0.03	241 ± 7	244 ± 2	9.98 ± 0.04	5.15	250 ± 2	15.5
$UC_{Er}@RB$	0.174 ± 0.002	1.5 ± 0.1	0.35 ± 0.03	258 ± 3	247 ± 4^b	3.58 ± 0.04	3.73	165 ± 2	6.1

^{a} SD: standard deviation of the measurement. ^{b} Average lifetime of a biexponential fitting ($\tau_1 = 46 \pm 2(8\%)$; $\tau_2 = 265 \pm 3(92\%)$). ^{c} Extrapolated from two values.

goes a slight hypsochromic shift (560 nm *vs.* 563 nm, respectively).

Xanthenic dyes form H-type aggregates.[48–53] For example, xanthenes are aggregated when encapsulated in cucurbit[8] uril.[54,55] The aggregation is evidenced by an increase in the relative absorption of the shoulder (absorption of the aggregates) as compared to the maximum absorption of the monomer. Although RB is a dianionic xanthenic dye that is highly soluble in polar solvents, it can also form H-type aggregates[51,53] in protic polar solvents,[51] in the presence of alkali metal ions[56,57] or by interaction with positively charged surfaces.[50,52,53,58–60] The formation of RB aggregates drastically reduced the emission quantum yield and also the quantum yield of singlet oxygen generation.[52] Control experiments have shown that RB does easily aggregate in DMF (see the ESI and Fig. S4†). In this case, for $UC_{Er}@RB$ and RB, the ratio between λ_{max} and the shoulder changes drastically (A_{560}/A_{522} = 2.5 and A_{563}/A_{522} = 3.8, respectively). In addition, the emission spectrum of RB in $UC_{Er}@RB$ is slightly red shifted (λ_{max} = 583 *vs.* 578 nm for RB) while maintaining an identical shape. The fluorescence quantum yield (Φ_F) of RB (0.42) is reduced to 0.17 when RB is anchored to the UCNP surface (different λ_{exc} values were tested from 510 to 560 nm) (Fig. 2b). Garcia *et al.*[54] reported a drastic reduction, similar to the one observed here, which was attributed to the self-deactivation effect due to π–π interactions in the aggregates. The increase in the A_{563}/A_{522}

absorption ratio, the bathochromic shift of RB emission in $UC_{Er}@RB$ and the Φ_F reduction indicate the presence of aggregates. This is consistent with the presence of aggregates in ground state due to the high RB concentration when functionalizing the UC_{Er} (see the ESI†).

A concentration of 3×10^{-6} M mg^{-1} UCNH has been calculated for RB (*ca.* 25 molecules/UCNP), considering an identical molar absorption coefficient for RB when anchored to the surface to that free in solution. Thus, only *ca.* 3% of the surface would be covered by RB (calculations in the ESI†). Even assuming that either the molar absorption coefficient of RB reduced by half due to the aggregation effect[49,50] or that the functionalization occurred exclusively on the lateral faces of the hexagonal prism,[61–63] the coverage was low (4.7% and 3.4%, respectively).

Note that a low functionalization does not exclude the presence of dye aggregates on the surface. In fact, dimer formation on positively charged surfaces has been observed previously, even when only 1% of the active sites were occupied.[64]

RB fluorescence lifetime (τ_F) was shorter in $UC_{Er}@RB$ (1.5 ns) than in solution (2.2 ns) (Table 1 and Fig. 2a). The singlet excited state can be deactivated by different pathways: fluorescence emission, intersystem crossing, non-radiative deactivation and/or possible energy transfer. The decrease in the Φ_F of RB in the UCNH together with a *ca.* 30% decrease in its lifetime indicated the presence of phenomena that effectively
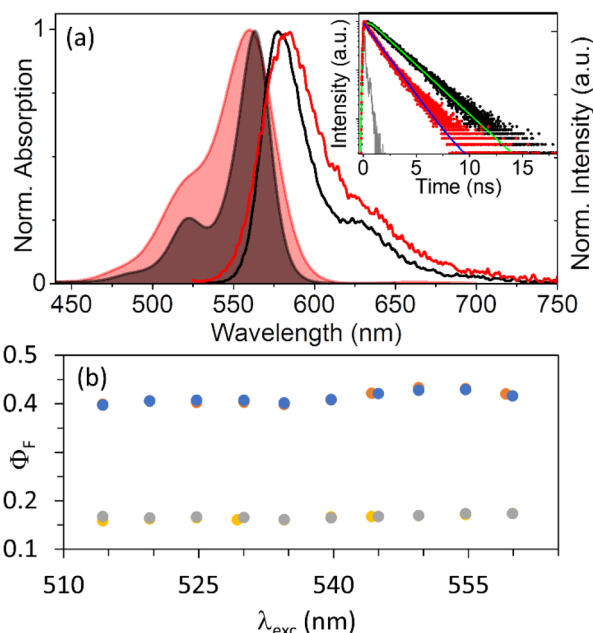
Fig. 2 (a) Normalized absorption (colored areas) and emission (lines, λ_{exc} = 522 nm) of RB (black) and UC$_{Er}$@RB (red). Raw attenuance data are shown in Fig. S3.† Inset: fluorescence lifetime kinetics (dots) and fitting (lines) of RB (black, 2.7 × 10^{-7} M) and UC$_{Er}$@RB (red, <1 mg mL^{-1}) under N$_2$; λ_{exc} = 560 nm, NKT laser 5.5 MHz; λ_{em} = 580 nm. (b) Fluorescence quantum yield of RB under air (blue dots) and N$_2$ (orange dots) and UC$_{Er}$@RB under air (grey dots) and N$_2$ (yellow dots) versus excitation wavelength (A = 0.1 at 560 nm).

quench the singlet excited state ^{1}RB. This can be attributed to different factors. One of them is RB aggregation, as mentioned above. Additionally, an improvement in the intersystem crossing efficiency when RB is anchored to the UCNP surface could be due to the heavy atom effect of the lanthanides,[31,65] or/and an energy transfer from ^{1}RB to the lanthanides (despite their low absorption coefficient). Both have been studied and are discussed in the following sections (see RB triplet state, internal conversion and energy transfer).

Internal conversion. The internal conversion quantum yield (Φ_{ic}) for free RB was estimated to be 0.13, according to eqn (1) valid for non-reactive molecules.[66]

$$\Phi_F + \Phi_{ISC} + \Phi_{IC} = 1 \qquad (1)$$

In contrast, the Φ_{ic} value of RB in UC$_{Er}$@RB was 0.48. A lower Φ_{ic} than the one obtained for free RB was expected for RB in UC$_{Er}$@RB, because RB was anchored to the UCNP surface. The hypotheses of ^{1}RB singlet deactivation due to the heavy atom effect of the UCNP and dye aggregation would result in an increase in the Φ_{isc}. Clearly this was not the case, thus leaving a possible energy transfer from ^{1}RB to Ln^{3+} as the preferred explanation. In this context, a new term ($\eta_{et}\Phi_{et}$), which considers the efficiency of the energy transfer (η_{et}) and the energy transfer quantum yield to the Ln^{3+} (Φ_{et}), should be added to eqn (1). If the Φ_{ic} values of RB in solution and in UC$_{Er}$@RB were identical, a contribution of 0.35 may be attribu-

ted to $\eta_{et}\Phi_{et}$. This photophysical pathway is discussed in the energy transfer section.

RB triplet state. Nanosecond-laser flash photolysis was used to register transient absorption spectra (Fig. 3a). The photophysical behavior of RB in DMF is similar to that reported in acetonitrile (ACN).[40] The RB triplet excited state (^{3}RB) was generated a few nanoseconds after the laser pulse and exhibited absorption bands at ca. 380, 470 and 610 nm. In the case of RB in solution, ^{3}RB subsequently evolved into the RB radical anion (RB$^{•-}$), which absorbs at ca. 440 nm and is long-lived (450 μs) (Fig. 3a). In contrast, when exciting RB in UC$_{Er}$@RB, ^{3}RB was exclusively generated, i.e., radical anion formation was clearly prevented. In a similar way, Baptista et al.[67] observed that when methylene blue aggregates were excited, they dissociated and formed a triplet identical to that of the monomer. Likewise, Kamat et al.[37] observed that rhodamine 6G aggregates on the surface of SiO$_2$ colloids formed only the triplet of the dye.

The kinetics of the singlet bleaching at 560 nm (τ_{Bl}) matched well with the absorption of the triplet at 610 nm (τ_T = 240–260 μs) and was very similar for free RB and RB in the UCNH (Fig. S6† and Table 1). However, the bleaching of RB at 560 nm was much weaker when RB is in the UCNH due to scattering and fitted a biexponential equation.

The intersystem crossing (or triplet formation) quantum yield (Φ_{isc}) of RB in UC$_{Er}$@RB was slightly lower (0.35), i.e., less ^{3}RB was formed as compared to RB (0.45, Table 1). As expected, RB Φ_{isc} values in aprotic polar solvents, such as DMF here reported or ACN (Φ_{isc} = 0.4),[68] were lower than in protic polar solvents (Φ_{isc} > 90%).[40]

Moreover, the rate constant for O$_2$ quenching of ^{3}RB, k_q(O$_2$) (Table 1 and Fig. S7†), revealed a fast process, close to a diffusion-controlled mechanism (k_{diff}(DMF) ≈ 8 × 10^9 M^{-1} s^{-1}).¶ Remarkably, this process was ca. three times slower for ^{3}RB in UC$_{Er}$@RB, probably due to the restricted mobility of RB when grafted to the UCNP and the formation of aggregates, which limited the diffusion rate.

Laser induced emission measurements showed that RB exhibits room temperature phosphorescence together with thermally activated delayed fluorescence, as previously reported for other xanthenic dyes, such as eosin.[69] The phosphorescence of ^{3}RB under N$_2$ began at ca. 670 nm and extended to ca. 1300 nm (vide infra) with a maximum at ca. 750 nm (755 and 753 nm for RB and UC$_{Er}$@RB, respectively; Fig. 3b). The phosphorescence intensity of RB in the UCNH was weaker and its lifetime (τ_P) was shorter than that of RB (Fig. 3c and Table 1). These results point out that there are other mechanisms that deactivate the ^{3}RB in the UCNH as compared to those of RB in solution. In addition, the weaker intensity of the delayed fluorescence of RB in UC$_{Er}$@RB emphasized, once again, the existence of a ^{1}RB deactivation process.

¶ Calculated from equation $k_{diff} = 8RT·10^3/(3\eta)$, R being the gas constant, T being the temperature and η being the viscosity of the solvent.[75]
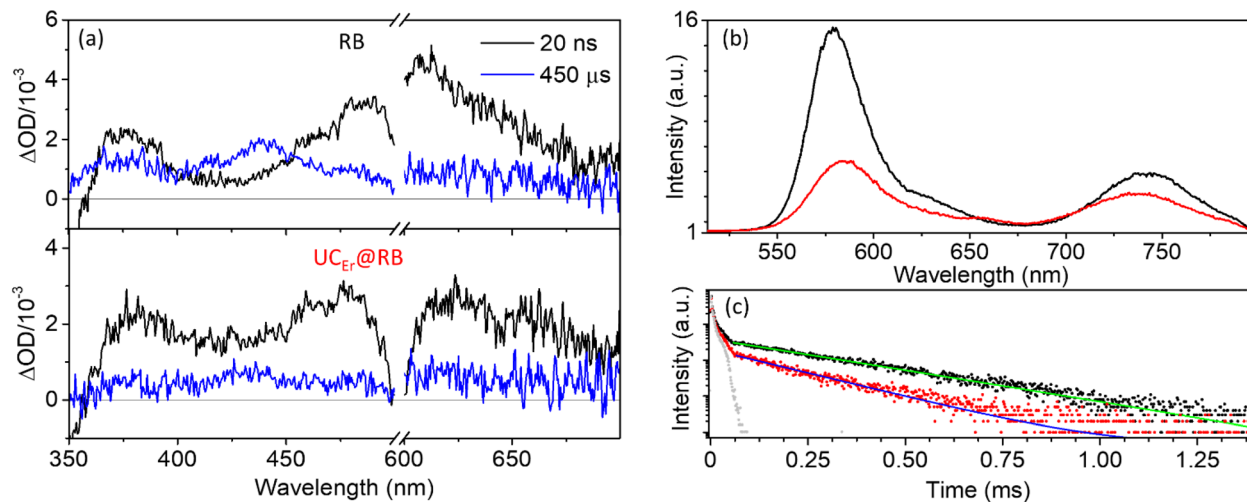
Fig. 3 (a) Transient absorption spectra of (top) RB and (down) UC_{Er}@RB recorded 20 ns (black) and 450 μs (blue) after the laser pulse under N_2 (λ_{exc} = 560 nm, A = 0.28 at 560 nm). (b) Laser-induced emission spectra of RB solution (black) and UC_{Er}@RB dispersion (red, A = 0.28 at 560 nm) 100 ns after the laser pulse (λ_{exc} = 560 nm) showing the phosphorescence and delayed emission of RB. (c) Kinetic profiles (dots) and fitting (lines) of RB (black, 1.6 × 10^{-5} M) and UC_{Er}@RB (red, 5 mg mL^{-1}) under N_2 (λ_{exc} = 560 nm, μF2 lamp; λ_{em} = 750 nm). Grey dots represent the IRF.

The NIR emission spectrum of RB (Fig. 4) showed that the tail of the phosphorescence lengthened up to *ca.* 1300 nm, while under air it was almost completely deactivated and the emission band characteristic of $^1O_2$ phosphorescence centered at 1275 nm was observed (scheme in Fig. S8†).

Energy transfer from RB to UC_{Er} in the UCNH. When RB in the UCNH was selectively excited, two intense new bands centered at 975 and 1550 nm were registered together with RB phosphorescence (Fig. 4). The band at 975 nm is attributed to the Yb^{3+} $^2F_{5/2} \rightarrow {}^2F_{7/2}$ transition (the Er^{3+} $^4I_{11/2} \rightarrow {}^4I_{15/2}$ transition could play a minor role due to the lower doping). The band at 1550 nm can be unequivocally attributed to the Er^{3+} $^4I_{13/2} \rightarrow {}^4I_{15/2}$ transition.

Upon energy transfer from RB, $^4F_{9/2}$ (655 nm) would be most likely the populated energy level of Er^{3+}. Control experiments showed that the emission bands at 975 and 1550 nm were weaker when exciting the UC_{Er} at 655 nm than the UC_{Er}@RB nanohybrid at 560 nm (Table S3†). Therefore, these

bands have been generated due to an efficient antenna effect from RB to the photoactive lanthanide ions in the UCNH (Fig. 1a).

Moreover, the emission intensities of these NIR bands at 975 nm (Yb^{3+} emission and ^{3}RB phosphorescence) and 1550 nm (Er^{3+} emission) were greatly influenced by the atmosphere (N_2/air).

The emission bands registered under air originated exclusively from an energy transfer process from ^{1}RB (pathway i in Fig. 1a), since ^{3}RB was efficiently deactivated under air (calculated O_2 quenching efficiency >0.99). Accordingly, the emission bands under an inert atmosphere are due to the energy transfer from ^{1}RB (46%) and ^{3}RB (54%) to the photoactive lanthanides (pathways i and ii in Fig. 1a). This result is consistent with *ca.* 50% reduction of the RB fluorescence and phosphorescence lifetimes.

The emission kinetic profiles at 975 nm and 1550 nm under N_2 were fitted to a biexponential decay function. At
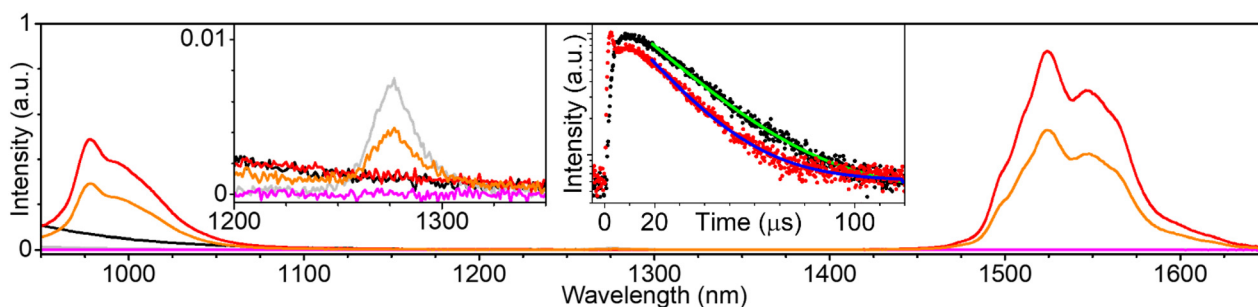

Fig. 4 NIR emission spectra of RB (1.6 × 10^{-5} M) under N_2 (black) and air (grey), UC_{Er} (5 mg mL^{-1}) under N_2 (pink) and UC_{Er}@RB (5 mg mL^{-1}) under N_2 (red) and air (orange); (λ_{exc} = 560 nm). RB solution and UC_{Er}@RB dispersion have identical absorbance (1.34 at 560 nm). Insets: (left) detail of the NIR emission spectra and (right) $^1O_2$ emission deactivation at 1275 nm of RB (black, 1.6 × 10^{-5} M) and UC_{Er}@RB (red, 5 mg mL^{-1}) under air (λ_{exc} = 560 nm, μF2 lamp).

975 nm, the biexponential behavior was due to the co-detection of two species: Yb^{3+} and ^3RB, a short one of 52 μs (65%) and a long one of 171 μs (35%) attributed to ^3RB phosphorescence. In fact, under air the kinetic profile fitted to a mono-exponential decay (48 μs; Fig. S9 and Table S4†). Similarly, at 1550 nm, Er^{3+} emission presented two components; the shortest component was quenched under air (209 μs *versus* 305 μs; Fig. S9 and Table S4†), again highlighting the participation of the ^3RB in the process.

In the presence of air, $^1O_2$ phosphorescence was observed at 1275 nm with the characteristic lifetime in DMF (19–23 μs; inset of Fig. 4). The relative intensity of this emission under air was lower for $UC_{Er}@RB$ (7.5×10^{-2} a.u. in RB *vs.* 4.3×10^{-2} a.u. in $UC_{Er}@RB$; Fig. 4). This result is attributed to a lower generation of singlet oxygen by triplet–triplet energy transfer from ^3RB on the surface of the UCNP as compared to RB in solution. Consequently, if the final purpose of the UCNH were to efficiently generate $^1O_2$ (*e.g.*, for photodynamic therapy), the decrease of Φ_{isc} and $k_q(O_2)$ will dramatically influence the performance of the UCNH.

Photophysics of UC_{Er} in the UCNH

Upon NIR excitation at 980 nm, UC_{Er} transfers energy to RB in $UC_{Er}@RB$. Note that high chromophore absorption (despite low concentrations of UCNP) can produce secondary inner-filter effects or/and emission self-absorption that modify the shape of the emission spectrum. It is convenient to prepare diluted dispersions. Fig. 5a shows the emission spectrum of UC_{Er} and $UC_{Er}@RB$ at 1 mg mL^{-1} and at 5 mg mL^{-1} in which the inner-filter effect for $UC_{Er}@RB$ can be appreciated.

UC intensity and lifetimes were not affected by the gas atmosphere (N_2 or air). As previously reported, in the UCNH, the relative intensity of the UCNP emission affected by RB

absorption (520–540 nm) decreased slightly as compared to the UC_{Er} emission (Fig. 5a), and a new emission centered at 584 nm appeared. This new band can be attributed to the sensitized emission of RB from the Er^{3+} of the UCNP, since it presents a lifetime in the order of the UC emissions of the Er^{3+} (51 μs; Table 2) in comparison to the conventional fluorescence of RB by direct excitation (1.5 ns). Note that the broad-emission tail of RB emission overlaps with the Er^{3+} emission at 655 nm (therefore, the Er^{3+} emission intensity increased in Fig. 5a).

Likewise, the presence of RB in the UCNH produced a slight reduction in the lifetime of the bands affected by RB absorption with respect to the precursor UC_{Er} (Table 2 and Fig. S10†). Although the presence of the dye on the surface of the UCNP did not seem to greatly affect either the relative intensities of the Er^{3+} UC emissions or its deactivation kinetics, it did affect the overall performance of the UC process. The presence of the dye reduced *ca.* 50% of the upconversion quantum yield (UCQY) of the UCNH with respect to the UC_{Er} (Table 2 and Fig. 5b). This is an expected result because more non-radiative deactivation phenomena will be possible by adding more electronic states to the system (with RB).

The ^3RB generation sensitized by UC emissions was not observed by transient absorption spectroscopy at 980 nm (5 mJ per laser pulse). Likewise, an attempt was made to record the emission of $^1O_2$ in a dispersion of UCNH bubbled with O_2 for 20 minutes, but no signal could be detected. Although it has been widely reported that PS-functionalized UCNPs are capable of generating ROS,[44,70–74] the sensitized formation of ^3RB and $^1O_2$ could not be spectroscopically observed under our experimental conditions, probably because the instrumentation is not sensible enough to detect these species for our system.
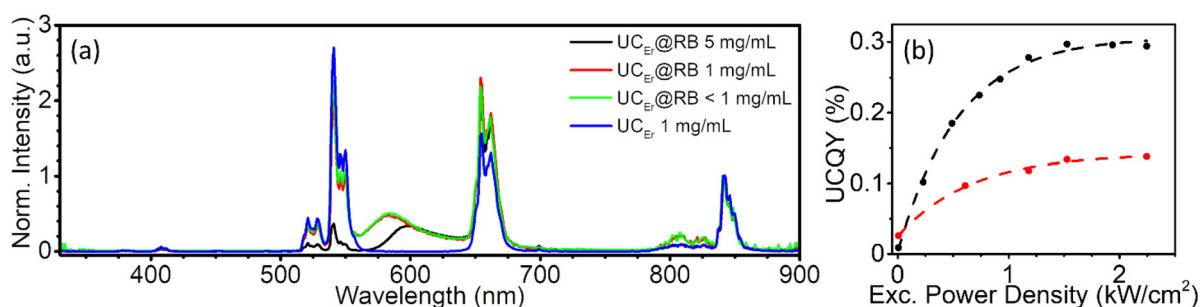

Fig. 5 (a) 841 nm-normalized corrected UC emission spectra of UC_{Er} and $UC_{Er}@RB$ dispersions at different concentrations (λ_{exc} = 980 nm; I = 2.1 W cm^{-2}). (b) Power density dependency of absolute UCQY for UC_{Er} and $UC_{Er}@RB$ dispersions in DMF (5 mg mL^{-1}).

Table 2 UC emission properties of UC_{Er} and $UC_{Er}@RB$ in DMF under an N_2 atmosphere (λ_{exc} = 980 nm). Kinetics fitting parameters are in Table S4†

Sample	$\tau_{525} \pm SD^a$ (μs)	$\tau_{540} \pm SD^a$ (μs)	$\tau_{600} \pm SD^a$ (μs)	$\tau_{655} \pm SD^a$ (μs)	UCQY$_{sat} \pm SD^{a\ b}$
UC_{Er}	85.9 ± 0.1	85.7 ± 0.1	—	205 ± 9	0.29 ± 0.1
$UC_{Er}@RB$	59.5 ± 0.1	59.3 ± 0.1	51.3 ± 0.1	202 ± 5	0.14 ± 0.1

^{a} SD: standard deviation. ^{b} UCQY in a saturation regime at 2.24 kW cm^{-2}, 5 mg mL^{-1} dispersion.

Conclusions

In summary, the results here described shed light on unresolved questions when functionalizing an UCNP with a xanthenic dye, such as RB. The photophysics of RB can be drastically affected by the aggregation and interaction with the UCNP surface and the presence of photoactive lanthanide cations (Yb^{3+}, Er^{3+}) doping the UCNP matrix.

The low functionalization degree and RB aggregation in $UC_{Er}@RB$ are attributed to the high concentration of RB in DMF used for functionalization. Equally important, the dynamics of RB excited states were roundly changed: Φ_F and Φ_{isc} decreased (specially the Φ_F) and both ^1RB and ^3RB excited states were deactivated by means of energy transfer processes from the dye to the photoactive lanthanides in the UCNPs (lower emission intensity and shorter fluorescence and phosphorescence lifetimes). As far as we know, this is the first experimental demonstration of the equal contribution of ^1RB and ^3RB to the antenna effect from RB to Yb^{3+} and Er^{3+}, which results in NIR-II emissions. Indeed, as previously reported for similar UCNHs, the UC emission spectra showed little influence on the intensity ratio of the Ln^{3+} emission bands for the nanohybrid (when avoiding the secondary inner filter effect), and a new sensitized long-lived emission from RB was detected due to a resonant energy transfer from Er^{3+} to ^1RB. Moreover, the absolute external UCQY of the system decreased to half as compared to that of the pristine UCNP. Therefore, rather than a synergistic or additive effect, in this UCNH, we observed an antagonistic effect which limits its potential application as a bioimaging or $^1O_2$ generation agent.

All in all, it was demonstrated that the dye photophysics in solution cannot be taken for granted when functionalizing UCNPs, and every case should be studied in advance to ensure a synergistic rather than an antagonistic effect. This knowledge is of utmost importance to design efficient functional UCNHs. In the case of designing bioimaging probes, a reduction in the dye Φ_F will be an additional limitation to the low UCQY of the UCNP. Similarly, as shown here for the $UC_{Er}@RB$ nanohybrid, if the aim is to generate $^1O_2$, the reduction in the dye Φ_{isc} together with the slower diffusion of the colloid will negatively affect the $^1O_2$ quantum yield. In this example, the doping of the UCNP with Gd^{3+} may be a plausible and rational solution. In any case, the effects of Gd^{3+} doping, UCNP size, dye loading, and concentration used for the functionalization process, the distance between Ln^{3+} and dyes, and chromophores with different ratios of singlet/triplet need to be studied in the future to design UCNHs.

Author contributions

Juan Ferrera-González: investigation, methodology, data curation, visualization, and writing – original draft; María González-Béjar: conceptualization, supervision, and writing – review & editing; Julia Pérez-Prieto: conceptualization, supervision, and writing – review & editing.

Conflicts of interest

There are no conflicts to declare.

Acknowledgements

References

1 F. Auzel, *Chem. Rev.*, 2004, **104**, 139–173.

2 G. Tessitore, G. A. Mandl, M. G. Brik, W. Park and J. A. Capobianco, *Nanoscale*, 2019, **11**, 12015–12029.

3 X. Li, F. Zhang and D. Zhao, *Chem. Soc. Rev.*, 2015, **44**, 1346–1378.

4 M. R. Hamblin, *Dalton Trans.*, 2018, **47**, 8571–8580.

5 M. González-Béjar, L. Francés-Soriano and J. Pérez-Prieto, *Front. Bioeng. Biotechnol.*, 2016, **4**, 47.

6 X. Zhu, J. Zhang, J. Liu and Y. Zhang, *Adv. Sci.*, 2019, **6**, 1901358.

7 B. Chen and F. Wang, *Trends Chem.*, 2020, **2**, 427–439.

8 W. Xu, X. Chen and H. Song, *Nano Today*, 2017, **17**, 54–78.

9 W. Xu, H. Liu, D. Zhou, X. Chen, N. Ding, H. Song and H. Ågren, *Nano Today*, 2020, **33**, 100892.

10 E. Andresen, U. Resch-Genger and M. Schäferling, *Langmuir*, 2019, **35**, 5093–5113.

11 F. Pini, L. Francés-Soriano, V. Andrigo, M. M. Natile and N. Hildebrandt, *ACS Nano*, 2023, **17**, 4971–4984.

12 L. Francés-Soriano, N. Estebanez, J. Pérez-Prieto and N. Hildebrandt, *Adv. Funct. Mater.*, 2022, **32**, 2201541.

13 J. Ferrera-González, M. González-Béjar and J. Pérez-Prieto, in *Dyes and Photoactive Molecules in Microporous Systems. Structure and Bonding*, ed. F. López Arbeloa, Springer, Cham, 2020, pp. 371–396.

14 X. Wang, R. R. Valiev, T. Y. Ohulchanskyy, H. Ågren, C. Yang and G. Chen, *Chem. Soc. Rev.*, 2017, **46**, 4150–4167.

15 Y. Liu, X. Meng and W. Bu, *Coord. Chem. Rev.*, 2019, **379**, 82–98.

16 A. Zhou, Y. Wei, B. Wu, Q. Chen and D. Xing, *Mol. Pharm.*, 2012, **9**, 1580–1589.

17 Q. Yuan, Y. Wu, J. Wang, D. Lu, Z. Zhao, T. Liu, X. Zhang and W. Tan, *Angew. Chem., Int. Ed.*, 2013, **52**, 13965–13969.

18 M. González-Béjar, M. Liras, L. Francés-Soriano, V. Voliani, V. Herranz-Pérez, M. Duran-Moreno, J. M. Garcia-Verdugo, E. I. Alarcon, J. C. Scaiano and J. Pérez-Prieto, *J. Mater. Chem. B*, 2014, **2**, 4554–4563.

19 K. Liu, X. Liu, Q. Zeng, Y. Zhang, L. Tu, T. Liu, X. Kong, Y. Wang, F. Cao, S. A. G. G. Lambrechts, M. C. G. G. Aalders and H. Zhang, *ACS Nano*, 2012, **6**, 4054–4062.

20 F. Chen, S. Zhang, W. Bu, Y. Chen, Q. Xiao, J. Liu, H. Xing, L. Zhou, W. Peng and J. Shi, *Chem. – Eur. J.*, 2012, **18**, 7082–7090.

21 X. Yang, Q. Xiao, C. Niu, N. Jin, J. Ouyang, X. Xiao and D. He, *J. Mater. Chem. B*, 2013, **1**, 2757–2763.

22 Y. Il Park, H. M. Kim, J. H. Kim, K. C. Moon, B. Yoo, K. T. Lee, N. Lee, Y. Choi, W. Park, D. Ling, K. Na, W. K. Moon, S. H. Choi, H. S. Park, S.-Y. Yoon, Y. D. Suh, S. H. Lee and T. Hyeon, *Adv. Mater.*, 2012, **24**, 5755–5761.

23 P. Zhang, W. Steelant, M. Kumar and M. Scholfield, *J. Am. Chem. Soc.*, 2007, **129**, 4526–4527.

24 A. M. Kotulska, A. Pilch-Wróbel, S. Lahtinen, T. Soukka and A. Bednarkiewicz, *Light: Sci. Appl.*, 2022, **11**, 1–14.

25 A. Pilch-Wróbel, A. M. Kotulska, S. Lahtinen, T. Soukka and A. Bednarkiewicz, *Small*, 2022, **18**, 2200464.

26 S. Melle, O. G. Calderón, M. Laurenti, D. Mendez-Gonzalez, A. Egatz-Gómez, E. López-Cabarcos, E. Cabrera-Granado, E. Díaz and J. Rubio-Retama, *J. Phys. Chem. C*, 2018, **122**, 18751–18758.

27 R. Marin, L. Labrador-Paéz, A. Skripka, P. Haro-González, A. Benayas, P. Canton, D. Jaque and F. Vetrone, *ACS Photonics*, 2018, **5**, 2261–2270.

28 O. Dukhno, F. Przybilla, M. Collot, A. Klymchenko, V. Pivovarenko, M. Buchner, V. Muhr, T. Hirsch and Y. Mély, *Nanoscale*, 2017, **9**, 11994–12004.

29 F. Pini, L. Francés-Soriano, N. Peruffo, A. Barbon, N. Hildebrandt and M. M. Natile, *ACS Appl. Mater. Interfaces*, 2022, **14**, 11883–11894.

30 S. Bhuckory, S. Lahtinen, N. Höysniemi, J. Guo, X. Qiu, T. Soukka and N. Hildebrandt, *Nano Lett.*, 2023, **23**, 2253–2261.

31 D. J. Garfield, N. J. Borys, S. M. Hamed, N. A. Torquato, C. A. Tajon, B. Tian, B. Shevitski, E. S. Barnard, Y. D. Suh, S. Aloni, J. B. Neaton, E. M. Chan, B. E. Cohen and P. J. Schuck, *Nat. Photonics*, 2018, **12**, 402–407.

32 S. Han, R. Deng, Q. Gu, L. Ni, U. Huynh, J. Zhang, Z. Yi, B. Zhao, H. Tamura, A. Pershin, H. Xu, Z. Huang, S. Ahmad, M. Abdi-Jalebi, A. Sadhanala, M. L. Tang, A. Bakulin, D. Beljonne, X. Liu and A. Rao, *Nature*, 2020, **587**, 594–599.

33 S. Han, Z. Yi, J. Zhang, Q. Gu, L. Liang, X. Qin, J. Xu, Y. Wu, H. Xu, A. Rao and X. Liu, *Nat. Commun.*, 2021, **12**, 1–9.

34 P. Zhang, J. Ke, D. Tu, J. Li, Y. Pei, L. Wang, X. Shang, T. Guan, S. Lu, Z. Chen and X. Chen, *Angew. Chem., Int. Ed.*, 2022, **61**, e202112125.

35 X. Wang, X. Wang, G. V. Baryshnikov, R. R. Valiev, R. Fan, S. Lu, H. Ågren and G. Chen, *Chem. Eng. J.*, 2021, **426**, 131282.

36 K. R. Gopidas and P. V. Kamat, *J. Phys. Chem.*, 1989, **93**, 6428–6433.

37 C. Nasr, D. Liu, S. Hotchandani and P. V. Kamat, *J. Phys. Chem.*, 1996, **100**, 11054–11061.

38 I.-I. S. Lim, F. Goroleski, D. Mott, N. Kariuki, W. Ip, J. Luo and C.-J. Zhong, *J. Phys. Chem. B*, 2006, **110**, 6673–6682.

39 V. Muhr, C. Würth, M. Kraft, M. Buchner, A. J. Baeumner, U. Resch-Genger and T. Hirsch, *Anal. Chem.*, 2017, **89**, 4868–4874.

40 L. Ludvíková, P. Friš, D. Heger, P. Šebej, J. Wirz and P. Klán, *Phys. Chem. Chem. Phys.*, 2016, **18**, 16266–16273.

41 M. C. DeRosa and R. J. Crutchley, *Coord. Chem. Rev.*, 2002, **233–234**, 351–371.

42 W. Liu, Y. Zhang, W. You, J. Su, S. Yu, T. Dai, Y. Huang, X. Chen, X. Song and Z. Chen, *Nanoscale*, 2020, **12**, 13948–13957.

43 F. Jin, J. Qi, D. Liu, Y. You, G. Shu, Y. Du, J. Wang, X. Xu, X. Ying, J. Ji and Y. Du, *J. Controlled Release*, 2021, **337**, 90–104.

44 X. Chen, Y. Zhang, X. Zhang, Z. Zhang and Y. Zhang, *Microchim. Acta*, 2021, **188**, 1–10.

45 Y. Wang, K. Liu, X. Liu, K. Dohnalová, T. Gregorkiewicz, X. Kong, M. C. G. Aalders, W. J. Buma and H. Zhang, *J. Phys. Chem. Lett.*, 2011, **2**, 2083–2088.

46 Z. Li and Y. Zhang, *Nanotechnology*, 2008, **19**, 16–21.

47 A. Dong, X. Ye, J. Chen, Y. Kang, T. Gordon, J. M. Kikkawa and C. B. Murray, *J. Am. Chem. Soc.*, 2011, **133**, 998–1006.

48 N. J. Hestand and F. C. Spano, *Chem. Rev.*, 2018, **118**, 7069–7163.

49 B. Mendes, S. Kassumeh, A. Aguirre-Soto, Q. Pei, B. Heyne and I. E. Kochevar, *Photochem. Photobiol.*, 2021, **97**, 718–726.

50 M. E. Daraio and E. San Román, *Helv. Chim. Acta*, 2001, **84**, 2601–2614.

51 D. Xu and D. C. Neckers, *J. Photochem. Photobiol., A*, 1987, **40**, 361–370.

52 E. Alarcón, A. M. Edwards, A. Aspée, C. D. Borsarelli and E. A. Lissi, *Photochem. Photobiol. Sci.*, 2009, **8**, 933–943.

53 H. B. Rodríguez, M. G. Lagorio and E. S. Román, *Photochem. Photobiol. Sci.*, 2004, **3**, 674–680.

54 P. Montes-Navajas, A. Corma and H. Garcia, *ChemPhysChem*, 2008, **9**, 713–720.

55 P. Montes-Navajas, M. González-Béjar, J. C. Scaiano and H. García, *Photochem. Photobiol. Sci.*, 2009, **8**, 1743–1747.

56 O. Valdes-Aguilera and D. C. Neckers, *J. Photochem. Photobiol., A*, 1989, **47**, 213–222.

57 O. Valdes-Aguilera and D. C. Neckers, *J. Phys. Chem.*, 2002, **92**, 4286–4289.

58 M. B. E. Turbay, V. Rey, N. M. Argañaraz, F. E. Morán Vieyra, A. Aspée, E. A. Lissi and C. D. Borsarelli, *J. Photochem. Photobiol., B*, 2014, **141**, 275–282.

59 Y. Litman, M. G. Voss, H. B. Rodríguez and E. S. Román, *J. Phys. Chem. A*, 2014, **118**, 10531–10537.

60 P. V. Kamat and W. E. Ford, *Chem. Phys. Lett.*, 1987, **135**, 421–426.

61 W. Ren, S. Wen, S. A. Tawfik, Q. P. Su, G. Lin, L. A. Ju, M. J. Ford, H. Ghodke, A. M. Van Oijen and D. Jin, *Chem. Sci.*, 2018, **9**, 4352–4358.

62 H. Na, K. Woo, K. Lim and H. S. Jang, *Nanoscale*, 2013, **5**, 4242–4251.

63 S. Lahtinen, A. Lyytikäinen, H. Päkkilä, E. Hömppi, N. Perälä, M. Lastusaari and T. Soukka, *J. Phys. Chem. C*, 2017, **121**, 656–665.

64 W. E. Ford and P. V. Kamat, *J. Phys. Chem.*, 1989, **93**, 6423–6428.

65 G. A. Hebbink, L. Grave, L. A. Woldering, D. N. Reinhoudt and F. C. J. M. Van Veggel, *J. Phys. Chem. A*, 2003, **107**, 2483–2491.

66 S. L. Murov, I. Carmichael and G. L. Hug, *in Handbook of Photochemistry*, Marcel Dekker, INC., New York, 2nd edn, 1993, pp. 1–53.

67 H. C. Junqueira, D. Severino, L. G. Dias, M. S. Gugliotti and M. S. Baptista, *Phys. Chem. Chem. Phys.*, 2002, **4**, 2320–2328.

68 F. Stracke, M. Heupel and E. Thiel, *J. Photochem. Photobiol., A*, 1999, **126**, 51–58.

69 C. A. Parker and C. G. Hatchard, *Trans. Faraday Soc.*, 1961, **57**, 1894–1904.

70 C. Wang, L. Cheng and Z. Liu, *Theranostics*, 2013, **3**, 317–330.

71 N. M. Idris, M. K. Gnanasammandhan, J. Zhang, P. C. Ho, R. Mahendran and Y. Zhang, *Nat. Med.*, 2012, **18**, 1580–1585.

72 C. Wang, H. Tao, L. Cheng and Z. Liu, *Biomaterials*, 2011, **32**, 6145–6154.

73 D. Zhang, L. Wen, R. Huang, H. Wang, X. Hu and D. Xing, *Biomaterials*, 2018, **153**, 14–26.

74 Y. Liu, X. Meng and W. Bu, *Coord. Chem. Rev.*, 2019, **379**, 82–98.

75 S. L. Murov, I. Carmichael and G. L. Hug, *Handbook of Photochemistry*, Marcel Dekker, INC., New York, 2nd edn, 1993.